Research on a Fine Segmentation Algorithm for 3D Point Clouds of High-Density Overlapping Cucumber Canopies in Solar Greenhouses

Huayang Wang, Jiayuan Li, Maolin Hou, and Yuntao Ma

***Abstract*—To address the challenges in solar greenhouses where cucumber canopy point clouds are highly dense, leaves exhibit severe overlap, and inter-plant adhesion is pronounced, resulting in insufficient accuracy and poor robustness of traditional point cloud segmentation algorithms, this study proposes a comprehensive cucumber hierarchical segmentation framework (Cuc-HiSeg) for terrestrial laser scanning (TLS) point clouds, enabling high-precision segmentation from population level to individual plants and further to leaves. High-resolution three-dimensional (3D) point cloud data of cucumber canopies at the seedling, early flowering, and fruiting stages were collected using TLS. For segmentation from population to individual plants, an improved hierarchical density-based spatial clustering of applications with noise (HDBSCAN) algorithm integrating *k*-dimensional tree (KD-tree) optimization and secondary clustering with mean shift was developed, improving the F1-score by 0.7%, 5.0%, and 8.0% across the three growth stages compared with the original algorithm. For leaf segmentation, a leaf point cloud data augmentation algorithm named CuLeafExpander was proposed to enhance the generalization capability of deep learning models. Experimental results demonstrate that the improved HDBSCAN and region-growing (RG) algorithms attained F1-scores above 91.9% and 93.9%, respectively. The proposed Cuc-HiSeg provides technical support for efficient processing of crop point clouds and advances digital crop phenotyping and intelligent greenhouse management.**

***Index Terms*—Solar greenhouse, cucumber canopy, point cloud segmentation, hierarchical density-based spatial clustering of applications with noise (HDBSCAN) algorithm, region-growing algorithm**

I. Introduction

FACILITY agriculture represents a core pathway to overcoming natural climatic constraints and achieving year-round balanced supply of agricultural products, and it is also a key driver in the process of agricultural modernization in China [1]. Among the various modes of facility agriculture, solar greenhouses, characterized by their low cost and high energy efficiency, have become the dominant platform for vegetable production in northern cold regions, with continuously increasing planting scale and industrial value [2]. As one of the most widely cultivated and economically valuable vegetable crops in solar greenhouses, cucumber (*Cucumis sativus* L.) ranks first in the world in terms of annual sown area and total production [3]. The three-dimensional (3D) structure of the crop canopy directly influences light interception efficiency, canopy light distribution, and overall photosynthetic efficiency, thereby exerting a significant impact on crop yield formation, quality improvement, and resource utilization efficiency—key goals of modern facility agricultural production. The size and orientation of cucumber leaves [4, 5], as well as the morphological structure of individual plants [6, 7], can significantly alter internal canopy light distribution and resource use efficiency, further highlighting the practical significance of accurately characterizing cucumber canopy 3D structure for guiding field management practices and promoting precise and intelligent production of cucumber. Therefore, accurately characterizing the 3D structure of cucumber canopies is crucial for improving quality and efficiency in the cucumber industry and has become a research hotspot in the intelligent development of facility agriculture [8].

Point cloud data acquisition constitutes the fundamental prerequisite for digitizing the 3D structure of crop canopies, and current acquisition approaches for crop point clouds exhibit diversified characteristics. Depth camera-based acquisition methods are cost-effective and easy to operate, making them suitable for high-precision point cloud collection within small areas [9, 10]. Multi-view stereo (MVS) combined with structure from motion (SfM) reconstructs 3D point clouds by capturing two-dimensional images from multiple perspectives [11–13]. Although this method can accurately obtain the structure of individual plants, it is time-consuming and labor-intensive, and often requires specific planting configurations. With the rapid advancement of sensing technologies, light detection and ranging (LiDAR), an active remote sensing technique, has emerged prominently due to its high level of automation and rapid data acquisition capability [14–16]. LiDAR can efficiently acquire large-scale crop point cloud data while minimizing canopy disturbance, making it particularly suitable for large-scale agricultural production environments [17]. Terrestrial laser scanning (TLS), as a major application form of LiDAR, enables non-contact acquisition of massive 3D coordinate points and has been widely applied in marine monitoring [18], atmospheric research [19], disaster prediction [20], and autonomous driving [21]. In precision

Manuscript received: 3 March 2026; revised: 20 April 2026; accepted: 23 April 2026. *(Corresponding author: Yuntao Ma.)*

Citation: H. Wang, J. Li, M. Hou, and Y. Ma, Research on a fine segmentation algorithm for 3D point clouds of high-density overlapping cucumber canopies in solar greenhouses, *Int. J. Intell. Control Syst.*, 2026, 31(2), 137–148.

Huayang Wang, Jiayuan Li, Maolin Hou, and Yuntao Ma are with School of Land Science and Technology, China Agricultural University, Beijing 100091, China (e-mail: why_202203@163.com; lijiayuan2000@126.com; harmony_vip@163.com; yuntao.ma@cau.edu.cn).

Digital Object Identifier 10.62678/IJICS202606.10322

agriculture, TLS preserves the spatial morphology and topological relationships of leaves and stems [22], and has become a powerful tool for reconstructing 3D crop canopy structures [23–25]. For instance, Jin et al. [26] utilized TLS data to achieve precise segmentation of maize stems and leaves and to extract phenotypic parameters, demonstrating strong adaptability across maize plants of varying heights and densities. Lau et al. [27] scanned tropical trees using TLS, successfully reconstructed branch architectures, accurately identified branching orders, and achieved a branch length reconstruction accuracy of 87%. Murray et al. [28] quantified structural complexity in orchard trees using TLS, providing critical data support for yield estimation. Wu et al. [29] characterized the canopy structure of rapeseed using TLS and verified its high efficiency in extracting leaf area index (LAI). These studies collectively confirm that TLS possesses irreplaceable advantages in fine-scale digitalization of crop organs and 3D reconstruction of canopy structures, providing high-precision data input for phenotypic analysis. However, the enclosed and high-density planting environment of solar greenhouses poses severe challenges to effective TLS point cloud processing, as intertwined branches lead to significant noise interference, difficulty in separating targets from background, and blurred individual boundaries [30]. As a result, point cloud segmentation has become a critical bottleneck restricting the practical implementation of subsequent phenotypic analysis, underscoring the necessity of optimizing TLS point cloud processing techniques for solar greenhouse scenarios.

Traditional point cloud segmentation methods primarily analyze and process the geometric features and spatial relationships of point cloud data to partition them into different regions or objects, including model fitting-based methods, clustering-based methods [31], and region-growing (RG)-based methods [32]. Among these approaches, traditional clustering algorithms (e.g., Euclidean clustering (EC)) are extensively employed for crop point cloud segmentation owing to their computational efficiency. However, they exhibit inherent limitations when applied to the complex canopy architectures of solar greenhouse cucumbers. These methods rely heavily on predefined distance thresholds; in dense, overlapping canopy environments, suboptimal thresholding frequently results in over-segmentation (where a single plant or leaf is fragmented into discrete point cloud clusters) or under-segmentation (where adjacent plants are erroneously merged into a single cluster), thereby compromising the accuracy of downstream individual plant and leaf extraction. Although the hierarchical density-based spatial clustering of applications with noise (HDBSCAN) algorithm eliminates the need for manual parameter tuning, it remains inadequate for resolving the severe inter-plant adhesion typical of greenhouse cucumber canopies. The intricate entanglement of vines and overlapping foliage creates a continuous density distribution across adjacent plants, preventing HDBSCAN from delineating distinct inter-plant boundaries and leading to cross-plant mis-segmentation. Similarly, region-growing methods, which leverage geometric features such as normal vectors and curvature for segmentation, are hindered by point cloud incompleteness and leaf occlusion. The thin, irregular morphology of cucumber leaves often results in fragmented data during TLS acquisition, while severe leaf overlap confounds feature similarity assessments. Consequently, these methods struggle to segment compound leaf clusters effectively, frequently failing to separate overlapping leaf margins or improperly merging adjacent leaves.

In recent years, deep learning-based point cloud segmentation approaches have continuously evolved and been optimized, with their applications in crop point cloud segmentation becoming increasingly widespread. Zarei et al. [33] proposed PlantSegNet for instance segmentation of sorghum leaves grown in outdoor fields and created a large number of sorghum digital twin models to generate a large-scale synthetic dataset for training. By validating the model with both synthetic and real data, PlantSegNet achieved a mean precision of 69.0% on the real sorghum dataset. Chen et al. [34] employed an unmanned aerial vehicle (UAV)-based airborne LiDAR platform to collect cotton canopy point clouds and augmented the dataset through rotation, translation, random downsampling, and point order shuffling. Using the deep neural network PointNet++ for semantic segmentation of the original data, they extracted individual cotton plants with an extraction accuracy of 86.3%. However, deep learning-based segmentation methods still exhibit significant limitations when applied to TLS point clouds of solar greenhouse cucumber canopies. First, these methods heavily depend on large-scale, high-quality annotated point cloud datasets. Nevertheless, the thin, irregular, and highly overlapping nature of cucumber leaves leads to extremely high annotation costs and prolonged annotation cycles, making it challenging to construct large-scale annotated datasets covering different growth stages of cucumber. Second, existing annotated datasets are often confined to specific growth stages or planting densities, resulting in insufficient model training, weak generalization ability, and limited segmentation robustness in practical applications. For example, models trained on cucumber seedling stage data often fail to accurately segment dense canopies at the fruiting stage and struggle to adapt to the dynamic changes of cucumber canopies.

Compared with field crops, solar greenhouse cucumbers adopt a vine-training cultivation mode, and their canopy undergoes significant dynamic changes from a sparse structure at the seedling stage to a dense and closed state at the fruiting stage. Moreover, the leaves are thin, morphologically irregular, and frequently overlapping, which further increases the difficulty of point cloud segmentation. Specifically, the unique cultivation mode and canopy characteristics of solar greenhouse cucumbers amplify the inherent flaws of traditional clustering, HDBSCAN, region-growing, and deep learning-based segmentation methods: over-segmentation/under-segmentation in traditional clustering, poor handling of inter-plant adhesion in original HDBSCAN, ineffective segmentation of compound leaf clusters in region-growing, and insufficient generalization and dataset scarcity in deep learning methods. These issues collectively hinder the accurate hierarchical segmentation of cucumber canopies from population to individual plants and further to leaves.

In summary, existing approaches have not yet established a full-process, high-precision segmentation framework tailored to TLS point clouds of solar greenhouse cucumber canopies, making it difficult to achieve hierarchical and accurate segmentation from population canopy to individual plants and further to leaves. This deficiency directly restricts the practical application of cucumber canopy 3D structure characterization in agricultural production, hindering the realization of precision management and yield/quality improvement in facility cucumber cultivation. To address this research gap, this study focuses on the core challenges of TLS point cloud segmentation for solar greenhouse cucumber canopies and constructs a three-level progressive segmentation framework encompassing population, individual plant, and leaf, termed Cuc-HiSeg. Specifically, an improved HDBSCAN algorithm integrating *k*-dimensional tree (KD-tree) optimization and mean shift secondary clustering is proposed to overcome the difficulty of separating individual plants within high-density population canopies. A cucumber leaf-oriented point cloud data augmentation algorithm, CuLeafExpander, is designed to effectively alleviate the scarcity of annotated datasets. Furthermore, an enhanced region-growing algorithm combining morphological optimization and K-Means++ secondary segmentation is developed to achieve high-precision extraction of leaf instances within individual plants. Through comprehensive algorithmic innovation across the entire workflow and systematic validation at multiple growth stages, this study aims to provide core technical support for the digital extraction of 3D cucumber canopy structures in solar greenhouses by laying a solid foundation for the accurate acquisition of key phenotypic parameters, further guiding precision field management measures, improving resource utilization efficiency, and increasing cucumber yield and quality, while also offering a reference pathway for the intelligent development of phenotypic analysis in facility crops.

II. Materials and Methods

A. Experimental Greenhouse and Data Acquisition

The experiment was conducted from September 2023 to December 2023 in a typical energy-saving solar greenhouse at Baiwang Plantation (Fig. 1), Haidian District, Beijing (40°07′ N, 116°29′ E). The greenhouse was 80.0 m long, 8.0 m wide, and 3.9 m high at the ridge; cucumbers were planted in double rows on north-south oriented ridges with a plant spacing of 30.0 cm and row spacing of 40.0 cm, totaling 55 ridges.

Fig. 1 Planting scenario of cucumber in the greenhouse.

The experiment used an FARO Focus terrestrial laser scanner to collect point cloud data at three growth stages: seedling stage (stage I: 30 September 2023, average canopy height 0.55 m), early flowering stage (stage II: 14 October 2023, average canopy height 1.17 m), and fruiting stage (stage III: 2 November 2023, average canopy height 1.79 m). The scanning parameters were set to one-quarter resolution, two-fold quality enhancement, and five-fold high dynamic range (HDR); a six-station scanning strategy (four corners and midpoints of the long sides) was adopted, with each station taking approximately 10 min.

For the collected TLS data, FARO SCENE 2023 software was employed for the registration and fusion of multi-station 3D point clouds, as illustrated in Fig. 2. Target spheres placed between the large ridges were used as reference objects to initially determine the relative positions of point cloud data within the field of view of each scanning station. The hybrid registration function was utilized to combine target sphere-based registration with point-to-point registration. After registration, the multi-station 3D point cloud data were already in the same coordinate system but might contain minor deviations or noise.

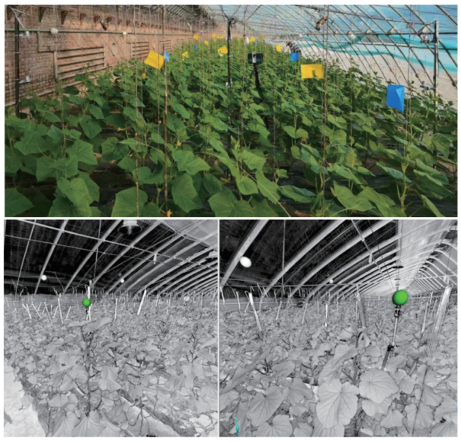

Fig. 2 Schematic diagram of point cloud scanning and processing.

Subsequently, the coordinates of the plant point clouds were corrected to ensure that they were perpendicular to the ground. Specifically, the rotation matrix from the z-axis of the current plant point clouds to the normal vector of the ground was calculated, and this rotation matrix was applied to the plant point clouds. The aligned point cloud data were then merged to ultimately generate a complete, high-density 3D point cloud model that could more comprehensively and accurately reflect the structure and morphology of the cucumber canopy.

Simultaneously, crop phenotypic parameters were collected: plant height, leaf length, and width were measured using a tape measure, and leaf inclination angle was measured using a digital protractor.

The workflow of the Cuc-HiSeg is shown in Fig. 3. The final individual-plant point cloud dataset contained 1274 cucumber plants, including 364 plants at the seeding stage, 468 at the early flowering stage, and 442 at the fruiting stage. The leaf point cloud dataset contained 2080 leaves; 80 plants

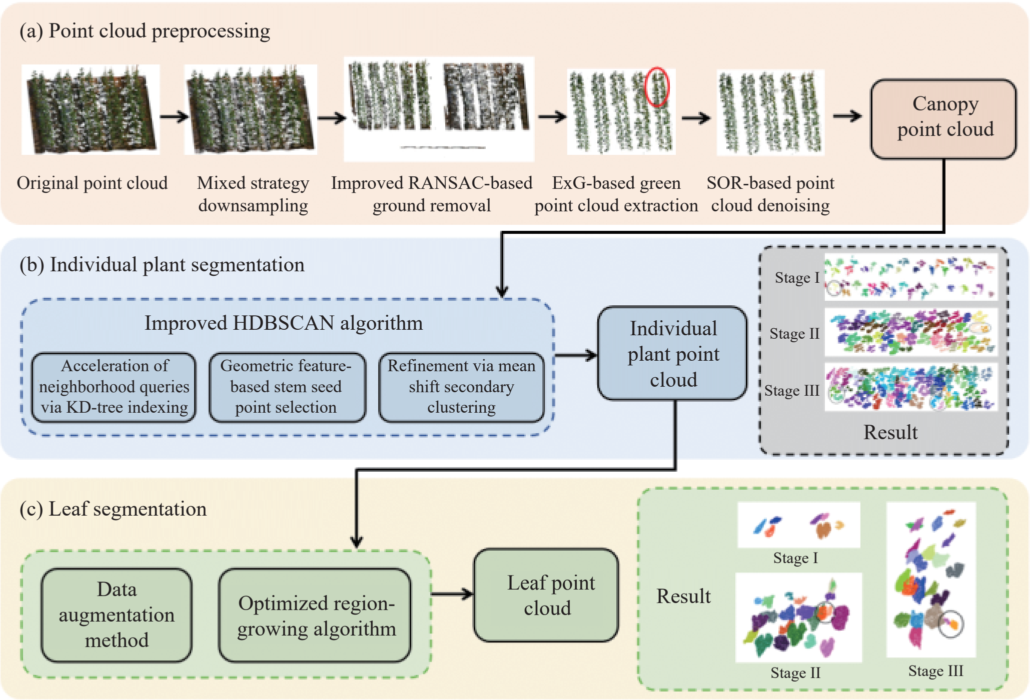

Fig. 3 Segmentation framework for cucumber canopy, individual plant, and leaf extraction from point cloud data. RANSAC is random sample consensus, ExG is excess green, and SOR is statistical outlier removal.

were selected at each growth stage, with an average of 4 leaves per plant at stage I, 8 leaves per plant at stage II, and 14 leaves per plant at stage III.

B. Preprocessing of Crop Point Cloud Data

To mitigate challenges arising from complex greenhouse backgrounds, high-density planting, which induces data redundancy and noise interference and ground-level contamination, this study implements a four-stage preprocessing pipeline to provide high-fidelity data support for subsequent segmentation tasks.

Initially, the local curvature of each point was calculated to preserve primary high-curvature morphological features, while voxel-based downsampling was applied specifically to low-curvature regions. Subsequently, the high-curvature feature points were integrated with the voxel-sampled points to achieve density-adaptive voxel sampling, yielding the finalized downsampled point cloud dataset.

For the ground-filtering phase, an optimized RANSAC algorithm was employed, wherein low-elevation candidate regions were identified via height histogram analysis and the optimal ground model was selected through slope constraints (calculating the angular deviation between the fitted plane and the horizontal surface). This approach effectively addresses the common limitation of the conventional cloth simulation filtering (CSF) algorithm, which frequently misclassifies low-hanging leaf points as ground, thereby ensuring robust terrain removal while preserving the integrity of the crop morphology.

Leveraging the multispectral capabilities of the FARO Focus laser scanner, the ExG index was utilized to extract vegetation regions from the RGB point cloud data, where R, G, and B represent the red, green, and blue color channel values, respectively. Based on the distinct spectral reflectance characteristics of chlorophyll in cucumber leaves, a mathematical model was constructed utilizing the RGB color channels. In this study, the raw RGB values were subjected to normalization to obtain the normalized color components r, g, and b.

$$r = \frac{R}{R+G+B} \tag{1}$$

Subsequently, the ExG index was applied to extract the crop point clouds, defined by Eq. (2).

$$\mathrm{ExG} = 2g - r - b \tag{2}$$

Finally, SOR filtering was implemented to eliminate outlier noise. Specifically, the Euclidean distance from each point to its k nearest neighbors was calculated, and points with a mean distance deviation exceeding the predefined threshold were removed to further enhance data purity.

C. Segmentation from Population to Individual Plants

In solar greenhouse environments, the dense arrangement of cucumber plants and severe leaf overlapping result in low neighborhood query efficiency and a tendency toward “under-segmentation” when applying the conventional HDBSCAN algorithm to large-scale point clouds. To address these issues, this study optimizes the algorithm across three dimensions: computational efficiency, seed point selection, and refined clustering. The overall workflow of the improved HDBSCAN algorithm was illustrated in Fig. 4.

a. Acceleration of Neighborhood Queries via KD-Tree Indexing

To process million-scale greenhouse population point clouds, a KD-tree spatial indexing structure was constructed to optimize neighborhood search efficiency. The optimized algorithm reduces the computational time complexity for core distance and mutual reachability distance from $O(n^2)$ to $O(n\log n)$. With the core distance d defined as the Euclidean distance from point p_i to its k-th nearest neighbor, this hierarchical estimation approach enables the autonomous identification of plant clusters with varying densities while maintaining high computational performance.

b. Geometric Feature-Based Stem Seed Point Selection

Since geometric adhesion caused by leaf-to-leaf contact is the primary cause of segmentation failure, principal component analysis (PCA) was introduced to calculate the local surface curvature of the point clouds. Exploiting the distinct linear topological structure and high curvature characteristic of cucumber stems, the algorithm identified high-curvature points to serve as "growth seed points". By utilizing the topological center (stem) rather than peripheral leaves as the clustering origin, physical isolation between adjacent plants was achieved at the geometric source, effectively resolving individual plant misclassification in high-density environments.

c. Refinement via Mean Shift Secondary Clustering

To address ambiguous boundary determination in overlapping regions following initial segmentation, the mean shift algorithm was implemented for fine-grained adjustment. Using the identified seed points as centroids, density center displacement iterations were performed via a Gaussian kernel function, with the search bandwidth set to 0.1 m (consistent with typical cucumber spacing in solar greenhouses). The algorithm iteratively updates positions toward local density maxima until convergence, forming independent density centers. This step enables precise attribution of overlapping leaf points, ensuring that each plant within the closed canopy was extracted completely and independently.

D. Individual Plant to Leaf Segmentation

To meet the requirements for leaf-level segmentation of individual cucumber plant point clouds, this study first expanded the sample size via data augmentation, evaluated the performance of deep learning architectures, and ultimately implemented a high-precision leaf segmentation method based on an optimized conventional RG algorithm.

a. CuLeafExpander Data Augmentation and Deep Learning Benchmark Testing

To address the high costs associated with 3D point cloud annotation and the limited scale and diversity of cucumber leaf datasets, while simultaneously evaluating the efficacy of deep learning models in leaf segmentation tasks, a structural-aware data augmentation algorithm was developed for dataset expansion, followed by comprehensive deep learning benchmark testing.

To address the limitations of existing datasets, a data augmentation algorithm specifically designed for cucumber

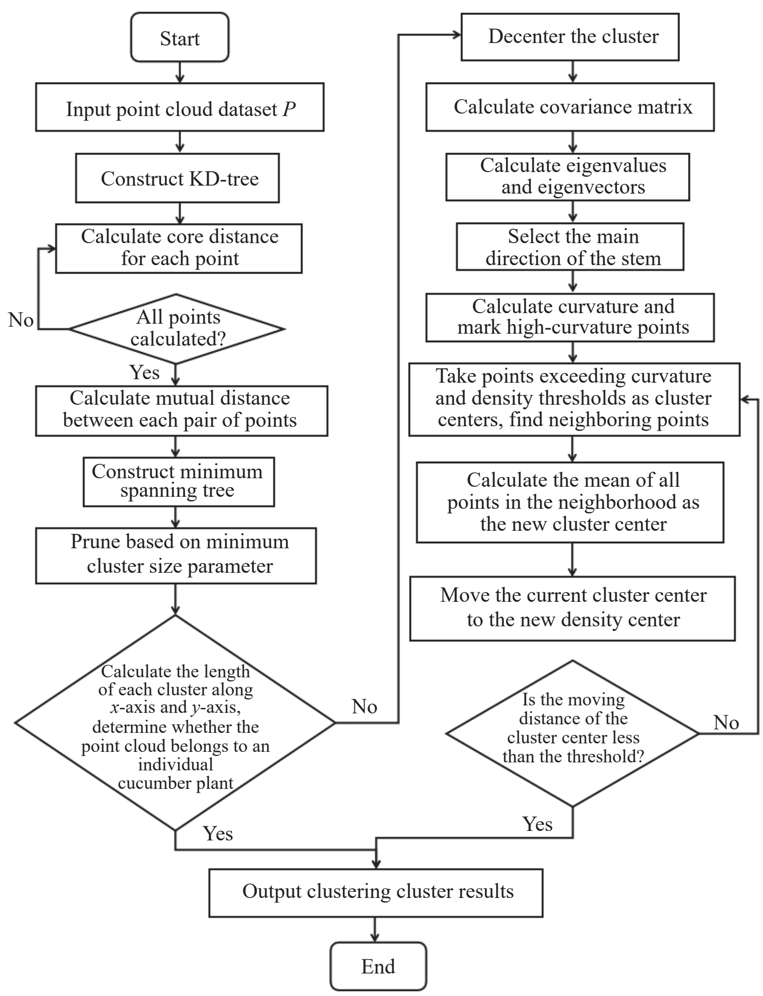

Fig. 4 Flowchart of the improved HDBSCAN algorithm.

leaf point clouds, termed CuLeafExpander, was proposed. The process began by segmenting individual plant point clouds into leaf and stem organs based on instance labels, followed by the application of a 3D convex hull algorithm to model the external boundary envelopes of individual leaf point clouds. Compared to the direct application of PCA to the entire leaf point cloud, the oriented bounding box (OBB) extraction method based on convex hull vertices effectively mitigated interference from internal leaf curling and incomplete holes. This approach allowed for a more precise determination of the primary and secondary axes representing leaf length and width, thereby establishing a reliable geometric baseline for subsequent data augmentation. Augmented samples that conform to realistic morphologies were generated through four strategies: dimensional transformation, angular rotation, stochastic edge perturbation, and point cloud density adjustment. The schematic representation of these augmentation strategies is illustrated in Fig. 5.

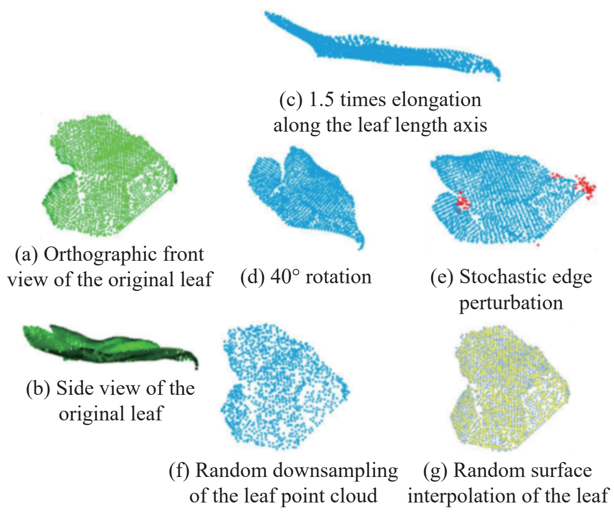

Fig. 5 Schematic diagram of data augmentation effects using CuLeafExpander.

The benchmark architectures PointNet++ and Point Transformer, widely recognized in the field of point cloud segmentation, were selected to conduct comparative testing within a compatible hardware and software environment. During the model training phase, optimized hyperparameters, including training epochs, loss functions, and optimizer settings, were established, with Dropout regularization integrated to mitigate overfitting. Quantitative evaluation and visualization analysis of the segmentation performance were subsequently performed using the CloudCompare toolkit.

b. Optimized Region-Growing Algorithm

Considering the substantial computational overhead and the prerequisite for extensive annotated datasets inherent in deep learning frameworks, conventional RG algorithms, which facilitate efficient, training-free segmentation by leveraging intrinsic geometric descriptors, offer superior alignment with the requirements for industrial viability and deployment. Consequently, this study developed an optimized iteration of the RG algorithm, specifically tailored for the leaf-level segmentation of individual cucumber plant point clouds. The complete workflow of the improved RG algorithm is illustrated in Fig. 6.

The conventional RG algorithm utilized low-curvature points as seeds and determined the merging of neighboring points based on normal vector similarity and curvature gradients. However, it exhibited poor performance when encountering isolated points, voids, and leaf overlapping in cucumber point clouds. The optimized algorithm first employed a KD-tree to accelerate neighborhood queries and implemented morphological dilation and erosion operations to fill voids, remove isolated noise, and refine leaf boundaries, thereby enhancing point cloud connectivity. Following the initial RG segmentation, overlapping multi-leaf composite clusters were identified by calculating the covariance matrix and eigenvalue ratios of the point sets to distinguish between individual and composite leaf clusters. Finally, the silhouette coefficient method was applied to automatically determine the optimal number of clusters for composite sets, which were then subjected to secondary segmentation via the K-Means++ algorithm to ensure a one-to-one correspondence between clusters and individual leaves. This hierarchical approach effectively resolved segmentation challenges induced by dense overlapping and structural incompleteness, significantly improving the robustness and precision of leaf segmentation across various growth stages.

To comprehensively evaluate the performance of the proposed Cuc-HiSeg, comparative experiments were conducted. EC is a well-established benchmark frequently employed for dense point cloud segmentation; thus, it was selected as the baseline for comparative experiments in this study.

E. Experimental Setup and Evaluation Metrics

For the deep learning-based segmentation, the individual plant point cloud dataset was partitioned into training, validation, and test sets using an 8:1:1 ratio. The proposed data augmentation framework, CuLeafExpander, was employed to perform structural transformations and diversity expansion on the training samples, resulting in the generation of 2036 additional synthetic plant instances. To ensure rigorous evaluation and prevent data leakage, these augmented data were exclusively incorporated into the training set; no augmentation was applied to the validation or test sets.

All deep learning experiments were carried out on two computing platforms with standardized configurations. For PointNet++, the implementation was conducted on a Windows 10 workstation equipped with an Intel(R) Core(TM) i9-9900KF CPU, 64 GB of RAM, and an NVIDIA GeForce RTX 3080 Ti GPU with 12 GB of video memory. The algorithm was developed in Python 3.7 with PyTorch 1.6, and the Open3D library was utilized for point cloud processing, visualization, and geometric analysis. For Point Transformer, experiments were performed on a high-performance server with a 20-core 40-thread CPU, 128 GB of RAM, and an NVIDIA GeForce RTX 3090 GPU with 24 GB of video memory, using Python 3.8 and PyTorch 1.11, together with Open3D. In addition, CloudCompare software was used for

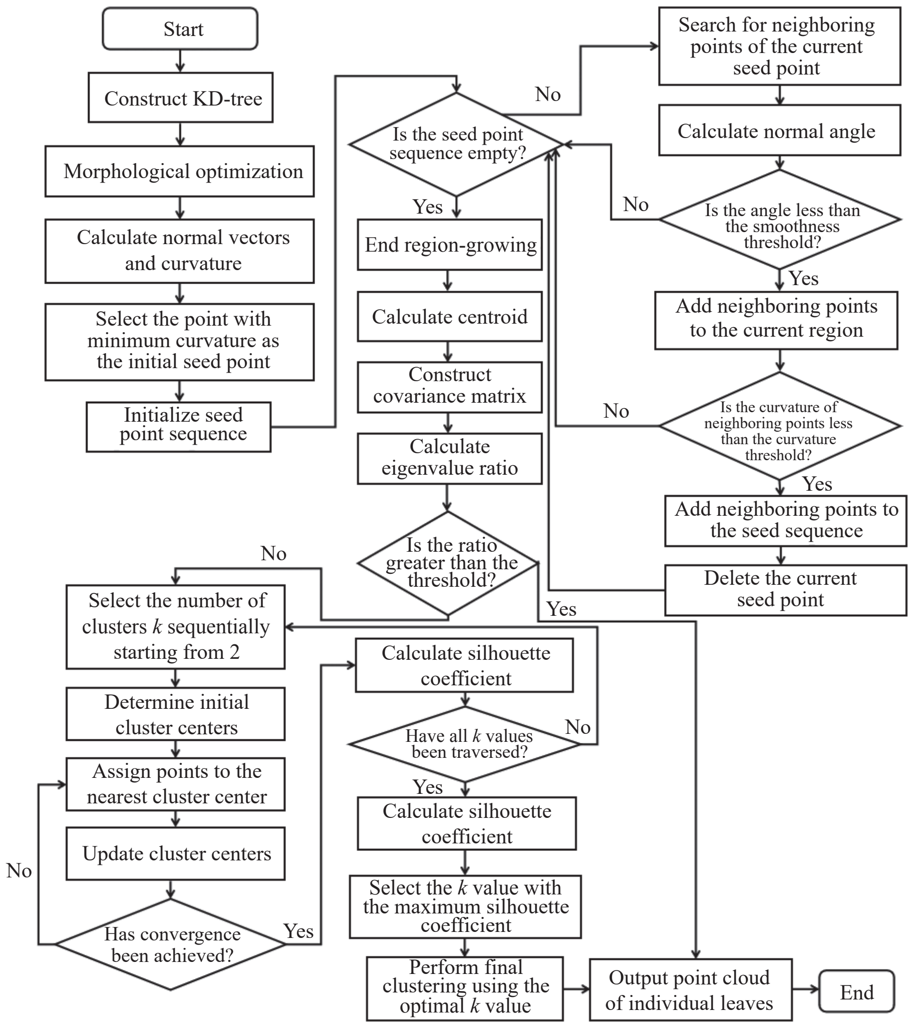

Fig. 6 Flowchart of the optimized region-growing algorithm.

visual inspection, point-to-point error evaluation, and quantitative comparison between original and augmented point clouds.

In the training phase, the number of epochs was set to 200. Cross-entropy loss was adopted to measure point-wise classification error, and the rectified linear unit (ReLU) activation function was used to enhance nonlinear feature learning. The Adam optimizer was applied with an initial learning rate of 0.001, followed by a 5% exponential decay after each epoch to improve convergence stability. Dropout with a rate of 0.5 was introduced in fully connected layers to reduce overfitting.

To quantitatively assess the efficacy of the optimized RG algorithm for cucumber plant point cloud segmentation in both individual plant and organ-level segmentation tasks, precision (P), recall (R), and F1-score were selected as the primary evaluation metrics in this study. Let true positive (TP) denotes the number of successfully matched pairs between predicted and ground truth instances; false positive (FP) represents the number of predicted instances that failed to match any ground truth; and false negative (FN) signifies the number of ground truth instances not correctly identified by any predicted instance. Accordingly, P represents the proportion of correctly matched instances among all segmented results, while R indicates the fraction of all ground truth instances that were successfully segmented and matched, as defined by Eqs. (3)–(5).

$$R = \frac{\mathrm{TP}}{\mathrm{TP}+\mathrm{FN}} \tag{3}$$

$$P = \frac{\mathrm{TP}}{\mathrm{TP}+\mathrm{FP}} \tag{4}$$

$$\text{F1-score} = \frac{2\times P\times R}{R+P} \tag{5}$$

III. RESULTS

A. Data Preprocessing Results

Following the four-stage preprocessing pipeline, high-fidelity cucumber canopy point cloud datasets were successfully generated from the raw TLS data across the three growth stages. The hybrid downsampling strategy effectively reduced the massive raw point cloud density while preserving key geometric features, particularly the linear structures of stems and the sharp margins of leaves. The improved RANSAC-based ground removal successfully isolated above-ground vegetation and accurately preserved low-hanging leaf clusters that are often misclassified by standard filters. Furthermore, the ExG-based extraction effectively removed non-vegetative background artifacts, and the SOR filtering eliminated discrete noise points. The resulting preprocessed point clouds exhibited significantly enhanced connectivity and reduced data redundancy, providing a standardized and clean geometric input for the subsequent hierarchical segmentation.

B. Population-to-Individual Plant Segmentation Results

After the four-stage preprocessing pipeline, high-fidelity cucumber canopy point cloud datasets were obtained at three growth stages for subsequent segmentation experiments. Segmentation performances of EC, original HDBSCAN, and the improved HDBSCAN were quantified using P, R, and F1-score (Table 1).

Table 1 Quantitative comparison of individual plant segmentation performance across three distinct growth stages.

Algorithm	P (%)	R (%)	F1-score (%)	Growth stage
EC	92.7	86.8	89.6	Stage I
	88.9	76.9	82.5	Stage II
	82.4	69.0	75.1	Stage III
HDBSCAN	95.8	93.4	94.6	Stage I
	94.4	82.7	88.1	Stage II
	92.6	76.7	83.9	Stage III
Improved HDBSCAN	95.7	94.8	95.3	Stage I
	92.4	93.8	93.1	Stage II
	90.5	93.2	91.9	Stage III

At stage I, plants were smaller, point cloud density was lower, and canopy structure was clear. The F1-score was 94.6% for the original HDBSCAN and 95.3% for the improved HDBSCAN. The improved HDBSCAN achieved an F1-score 0.7% higher than the original HDBSCAN. Both algorithms showed high segmentation accuracy with similar precision and recall values.

At stage II, plant height and canopy density increased, and point cloud overlap became more severe. The precision, recall, and F1-score of both algorithms decreased compared with stage I. The original HDBSCAN achieved a precision of 94.4% and a recall of 82.7%. The improved HDBSCAN achieved a precision of 92.4% and a recall of 93.8%. The F1-score was 88.1% for the original HDBSCAN and 93.1% for the improved HDBSCAN.

At stage III, plant height and point cloud density reached the maximum. The F1-scores of both algorithms decreased further compared with stage II. The original HDBSCAN obtained a precision of 92.6% and a recall of 76.7%. The improved HDBSCAN obtained a precision of 90.5% and a recall of 93.2%. Compared with the original HDBSCAN, the improved HDBSCAN showed a 2.1% lower precision but a 16.5% higher recall. The overall F1-score of the improved HDBSCAN reached 91.9%.

Visual comparisons (Figs. 7–9) showed over-segmentation in EC and under-segmentation in the original HDBSCAN, especially at stage III. The improved HDBSCAN reduced both over-segmentation and under-segmentation across all three stages.

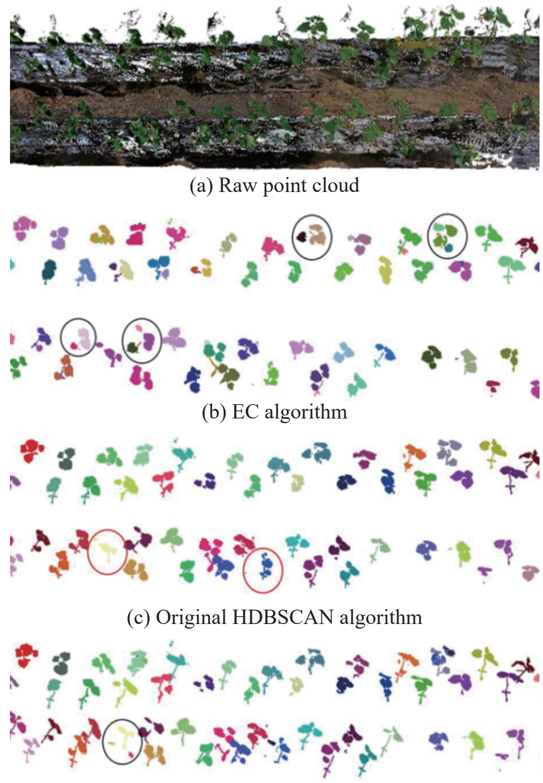

(a) Raw point cloud

(b) EC algorithm

(c) Original HDBSCAN algorithm

(d) Improved HDBSCAN algorithm

Fig. 7 Comparative result of individual plant segmentation during the seedling stage. Black circle indicates instance of over-segmentation (mis-segmentation), while red circle denotes instance of under-segmentation (missed detections).

C. Individual-to-Leaf Segmentation Results

a. CuLeafExpander Data Augmentation Results

To evaluate the effectiveness of the proposed data augmentation strategy, the leaf-level segmentation performance of two representative deep learning models (PointNet++ and Point Transformer) was assessed using precision, recall, and F1-score. The detailed comparative results, both before and after applying the CuLeafExpander augmentation, are summarized in Table 2.

The experimental results demonstrated that Point Transformer consistently outperformed PointNet++ across all three evaluation metrics, both before and after data augmentation. The CuLeafExpander algorithm improved segmentation performance at all three growth stages. The improvement in recall was greater than that in precision. The F1-score of PointNet++ increased by 6.2%, 6.0%, and 6.4% at stage I, stage II, and stage III, respectively. The F1-score of Point Transformer increased by 5.6%, 5.7%, and 5.7% at the three growth stages.

b. Optimized Region-Growing Segmentation Results

To perform a rigorous quantitative evaluation, 80 plant samples were randomly selected from each growth stage, totaling 240 plants and 2080 individual leaves across the three phenological periods. Table 3 provides a comprehensive comparison of the leaf-level segmentation metrics between the two algorithms throughout the three growth stages.

At stage I, no obvious differences in precision and recall

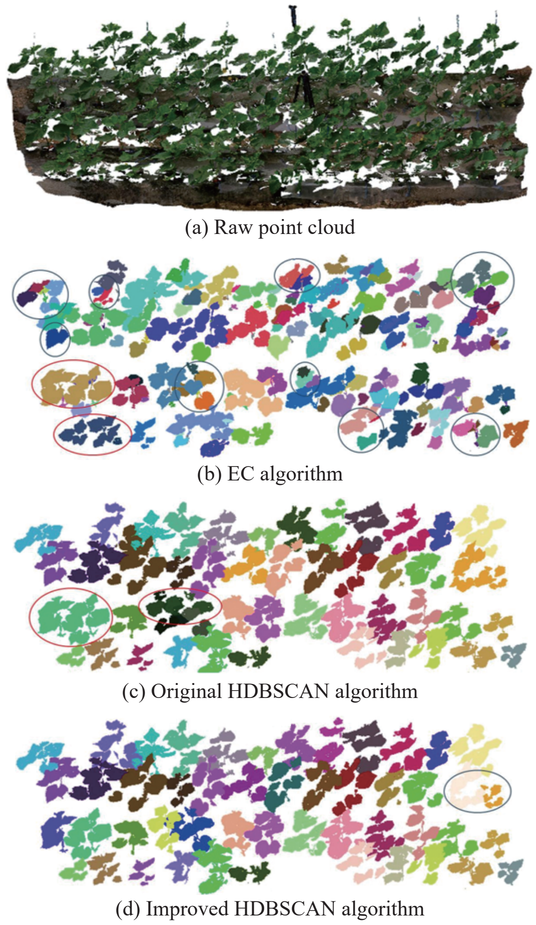

(a) Raw point cloud

(b) EC algorithm

(c) Original HDBSCAN algorithm

(d) Improved HDBSCAN algorithm

Fig. 8 Comparative visualization of individual plant segmentation result during the early flowering stage. Black circle indicates instance of over-segmentation (mis-segmentation), while red circle denotes instance of under-segmentation (missed detections).

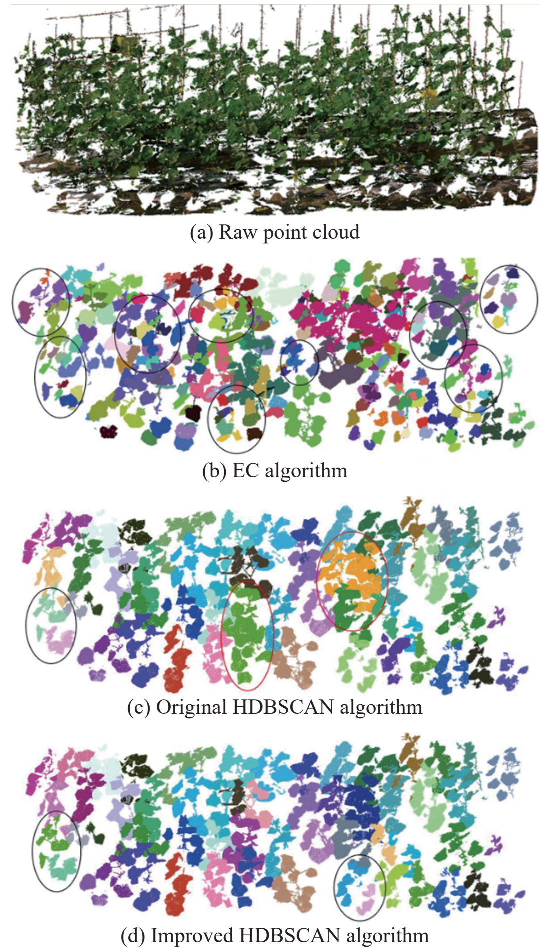

(a) Raw point cloud

(b) EC algorithm

(c) Original HDBSCAN algorithm

(d) Improved HDBSCAN algorithm

Fig. 9 Comparative visualization of individual plant segmentation result during the fruiting stage. Black circle indicates instance of over-segmentation (mis-segmentation), while red circle denotes instance of under-segmentation (missed detections).

were observed between the conventional RG algorithm and the optimized RG algorithm. The difference in F1-score between the two algorithms was 0.5%.

At stage II, leaf morphology became more complex, point cloud density increased, and partial leaf boundaries were unclear. The precision of the optimized RG algorithm was 1.3% lower than that of the conventional RG algorithm. The recall of the optimized RG algorithm was 5.0% higher than that of the conventional RG algorithm. The F1-score of the optimized RG algorithm was 2.1% higher than that of the conventional RG algorithm.

At stage III, the canopy was denser, leaf overlap was more severe, and partial point cloud loss occurred. The conventional RG algorithm merged incomplete leaf point clouds with adjacent leaves. The recall of the conventional RG algorithm decreased obviously. The recall of the optimized RG algorithm was 8.4% higher than that of the conventional RG algorithm. The F1-score of the optimized RG algorithm was 4.1% higher than that of the conventional RG algorithm. The performance gap between the two algorithms widened at stage III.

Visualization results (Fig. 10) showed that the optimized RG algorithm maintained clearer leaf boundaries and more stable segmentation under dense and occluded conditions.

IV. Discussion

The Cuc-HiSeg developed in this study effectively overcame the critical bottlenecks in cucumber point cloud segmentation within solar greenhouses, particularly the severe plant adhesion (clustering), the scarcity of annotated datasets, and the complexities associated with leaf overlapping and occlusion.

Firstly, at the population segmentation level, the improved HDBSCAN algorithm integrates KD-tree optimization and mean shift secondary clustering, achieving a superior balance between computational efficiency and segmentation accuracy. At the seedling stage with sparse and clear canopy structure, the proposed algorithm slightly improved the F1-score, which indicated that the mean shift module enhanced the ability to distinguish adjacent individual plants. In the early flowering stage with increased canopy density and overlap, the original HDBSCAN suffered from obvious under-segmentation and low recall, while the improved HDBSCAN maintained high precision and greatly elevated recall, showing stronger adaptability to dense point cloud environments. In the fruiting stage with the densest canopy and most severe adhesion, the improved HDBSCAN still achieved a high F1-score of 91.9%. Although precision decreased slightly, recall was greatly improved by 16.5% compared with the original algorithm,

Table 2 Comparative assessment of leaf-level segmentation performance with and without the CuLeafExpander data augmentation.

Augmentation status	Model	*P* (%)	*R* (%)	F1-score (%)	Growth stage
Before augmentation	PointNet++	79.1	60.4	68.5	Stage I
		76.2	59.8	67.1	Stage II
		74.3	58.8	65.6	Stage III
	Point Transformer	81.0	68.1	74.0	Stage I
		80.4	66.5	72.8	Stage II
		78.2	65.9	71.5	Stage III
After augmentation	PointNet++	81.8	68.8	74.7	Stage I
		78.2	68.6	73.1	Stage II
		76.7	67.9	72.0	Stage III
	Point Transformer	83.8	75.7	79.6	Stage I
		82.6	74.7	78.5	Stage II
		80.7	74.0	77.2	Stage III

Table 3 Performance comparison of leaf-level segmentation between conventional and optimized region-growing algorithms across three growth stages.

Algorithm	*P* (%)	*R* (%)	F1-score (%)	Growth stage
Conventional RG	95.2	93.7	94.5	Stage I
	95.6	89.5	92.4	Stage II
	96.8	83.8	89.8	Stage III
Optimized RG (proposed)	95.3	94.7	95.0	Stage I
	94.3	94.5	94.5	Stage II
	95.6	92.2	93.9	Stage III

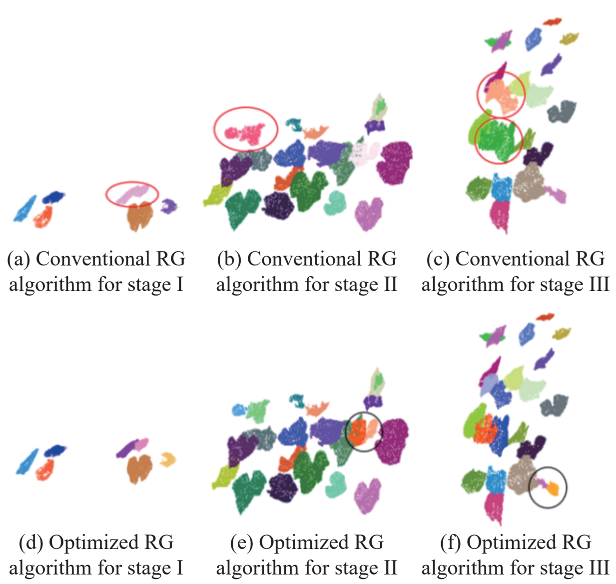

Fig. 10 Qualitative comparison of leaf-level segmentation result across three growth stages.

which meant that the problem of merging multiple plants into one was significantly alleviated. The above results confirmed that the improved HDBSCAN could effectively suppress under-segmentation in high-density and high-adhesion scenes, providing reliable individual plant extraction for greenhouse cucumber phenotyping.

Secondly, at the leaf instance segmentation stage, the CuLeafExpander data augmentation algorithm significantly improved the performance of deep learning models. Point Transformer performed better than PointNet++ in all growth stages, showing that its feature extraction ability was more suitable for complex leaf point cloud segmentation. After augmentation, the recall increased more significantly than precision, and the F1-scores of the two models were improved by approximately 5.6%–6.4%, which proved that CuLeafExpander effectively increased sample diversity and reduced missed detection. Nevertheless, deep learning methods were still limited by point cloud missing and complex leaf morphology, making it difficult to meet the requirements of high-precision leaf segmentation. The optimized region-growing algorithm achieved stable and high-precision leaf segmentation across the whole growth period. In the seedling stage, the algorithm performed similarly to the conventional RG, since leaves were scattered and regularly shaped. In the early flowering stage, the optimized RG reduced the merging of adjacent leaves, with recall increased by 5.0% and F1-score increased by 2.1%, showing stronger robustness for dense leaves. In the fruiting stage with severe overlap and point cloud loss, the conventional RG merged incomplete leaf clusters and caused a sharp drop in recall, while the optimized RG still maintained clear boundaries and stable output, with recall increased by 8.4% and F1-score increased by 4.1%. These results demonstrated that morphological optimization and K-Means++ secondary segmentation effectively overcame the interference of leaf overlap and point cloud defects, making the Cuc-HiSeg more suitable for fine leaf segmentation in complex greenhouse canopies.

Notably, high-precision point cloud segmentation paves the way for the construction of "digital crops". Accurate leaf instances and stem skeleton point clouds serve as the core geometric sources for developing functional-structural plant models [35, 36]. The refined canopy structural data derived from our segmentation can be directly integrated into light micro-climate simulations within solar greenhouses [37, 38], providing a digital basis for precision management strategies, such as supplemental lighting optimization and crop population layout adjustment. This aligns closely with the integrated "structure-function-regulation" research paradigm emphasized by Xu et al. [8] in their review of 3D simulation technologies.

Despite these promising results, several avenues for further optimization remain. First, the segmentation accuracy at the apical meristems requires further improvement, as these regions feature sparse point clouds and intricate structures that make them susceptible to over-segmentation or omission. Furthermore, future research should focus on deploying the proposed algorithm onto automated phenotyping platforms. By integrating multispectral and thermal infrared data with spatial localization algorithms, large-scale continuous monitoring can be achieved, thereby establishing a multidimensional perception system for crop growth. Finally, coupling these high-quality segmentation priors with advanced reconstruction techniques, such as 3D Gaussian splatting [39], can significantly enhance the fidelity and rendering efficiency of 3D canopy models. This synergy will provide robust foundational support for the intelligent upgrading of greenhouse digital twins and facility crop phenotyping.

V. Conclusions

To address the challenges of complex canopy structures and severe physical adhesion in solar greenhouse cucumbers, this study developed an effective three-stage Cuc-HiSeg for TLS point clouds. At the population level, an improved HDBSCAN algorithm integrating KD-tree spatial indexing and mean shift secondary clustering was proposed. This approach successfully overcame the dense overlapping characteristic of the full-closure stage, significantly improving individual plant recall and enabling the non-destructive isolation of densely planted crops.

At the leaf instance level, the structural-aware CuLeafExpander algorithm effectively mitigated the scarcity of annotated 3D data by geometrically expanding the diversity of complex leaf samples. Subsequently, an optimized RG algorithm enhanced with morphological constraints and K-Means++ initialization was employed, demonstrating superior robustness against leaf cavities and dense overlapping across all phenological stages. Ultimately, Cuc-HiSeg not only breaks through the bottlenecks of high-fidelity 3D parsing in dense canopies but also provides a robust geometric foundation for greenhouse digital twins and the deployment of digital crop phenotyping and intelligent greenhouse management.

Acknowledgment

This work was supported by the Beijing Smart Agriculture Innovation Consortium Project, China (No. BAIC10-2026) and the National Natural Science Foundation of China (No. 32372799).

References

[1] Z. Cao, S. Sun, G. Ma, A. Feng, K. Kang, G. Sun, and J. Li, Phase change materials for efficient thermal energy storage and its potential applications in sustainable facility agriculture: A critical review, *Renew. Sustainable Energy Rev.*, 2026, 225, 116169.

[2] P. Zhang, Q. Chen, Z. Chen, Y. Ren, W. Gao, J. Li, R. Lai, and X. Xie, Leaf color skewed-distribution parameters enhance the stability of phenotype-environment model across different growth cycles of cabbage, *Plant Growth Regul.*, 2026, 106(1), 10.

[3] H. Zhao, X. Zhai, L. Guo, Y. Yang, J. Li, C. Ren, K. Wang, X. Liu, R. Zhan, and K. Wang, Comparing protected cucumber and field cucumber production systems in China based on emergy analysis, *J. Clean. Prod.*, 2019, 236, 117648.

[4] Y. Y. Cho, S. Oh, M. M. Oh, and J. E. Son, Estimation of individual leaf area, fresh weight, and dry weight of hydroponically grown cucumbers (*Cucumis sativus* L.) using leaf length, width, and SPAD value, *Sci. Hortic.*, 2007, 111(4), 330–334.

[5] K. Kahlen, D. Wiechers, and H. Stützel, Modelling leaf phototropism in a cucumber canopy, *Funct. Plant Biol.*, 2008, 35(10), 876–884.

[6] B. Dechant, Y. Ryu, G. Badgley, Y. Zeng, J. A. Berry, Y. Zhang, Y. Goulas, Z. Li, Q. Zhang, M. Kang et al., Canopy structure explains the relationship between photosynthesis and sun-induced chlorophyll fluorescence in crops, *Remote Sens. Environ.*, 2020, 241, 111733.

[7] R. M. Deans, T. J. Brodribb, F. A. Busch, and G. D. Farquhar, Optimization can provide the fundamental link between leaf photosynthesis, gas exchange and water relations, *Nat. Plants*, 2020, 6(9), 1116–1125.

[8] D. Xu, J. Zhu, and Y. Ma, Advances in 3D simulation technology for solar greenhouse systems: A review, *Renew. Sustainable Energy Rev.*, 2026, 226, 116387.

[9] J. Wang, X. Li, Y. Zhou, H. Wang, and M. Li, Banana pseudostem width detection based on Kinect V2 depth sensor, *Comput. Intell. Neurosci.*, 2022, 2022, 3083647.

[10] D. Andújar, A. Ribeiro, C. Fernández-Quintanilla, and J. Dorado, Using depth cameras to extract structural parameters to assess the growth state and yield of cauliflower crops, *Comput. Electron. Agric.*, 2016, 122, 67–73.

[11] F. Hui, J. Zhu, P. Hu, L. Meng, B. Zhu, Y. Guo, B. Li, and Y. Ma, Image-based dynamic quantification and high-accuracy 3D evaluation of canopy structure of plant populations, *Ann. Bot.*, 2018, 121(5), 1079–1088.

[12] T. Duan, S. C. Chapman, E. Holland, G. J. Rebetzke, Y. Guo, and B. Zheng, Dynamic quantification of canopy structure to characterize early plant vigour in wheat genotypes, *J. Exp. Bot.*, 2016, 67(15), 4523–4534.

[13] C. Webster, M. Westoby, N. Rutter, and T. Jonas, Three-dimensional thermal characterization of forest canopies using UAV photogrammetry, *Remote Sens. Environ.*, 2018, 209, 835–847.

[14] M.-C. Jutras-Perreault, T. Gobakken, E. Naesset, and H. O. Ørka, Detecting the presence of natural forests using airborne laser scanning data, *Forest Ecosyst.*, 2023, 10, 100146.

[15] L. Weidner, G. Walton, and C. Phillips, Investigating the influences of precipitation, snowmelt, and freeze-thaw on rockfall in Glenwood Canyon, Colorado using terrestrial laser scanning, *Landslides*, 2024, 21(9), 2073–2091.

[16] G. Arseniou, D. W. MacFarlane, K. Calders, and M. Baker, Accuracy differences in aboveground woody biomass estimation with terrestrial laser scanning for trees in urban and rural forests and different leaf conditions, *Trees*, 2023, 37(3), 761–779.

[17] M. Pohorenec, M. Behún, P. Gnip, and A. Behúnová. LiDAR-based segmentation of tall vegetation, *Mobile Netw. Appl.*, 2026, to be published.

[18] L. Janowski, R. Wroblewski, M. Rucinska, A. Kubowicz-Grajewska, and P. Tysiac, Automatic classification and mapping of the seabed using airborne LiDAR bathymetry, *Eng. Geol.*, 2022, 301, 106615.

[19] V. G. Shemanin, V. A. Turkin, and V. E. Privalov, LiDAR measurements of hydrogen fluoride concentration in atmospheric boundary layer, *IOP Conf. Ser.: Earth Environ. Sci.*, 2021, 867, 012176.

[20] O. B. Ilesanmi, J. D. Rogers, and F. E. Oboh-Ikuenobe, Evaluation of geohazards in the Cape Girardeau area using LiDAR and GIS, Southeast Missouri, USA, *Environ. Earth Sci.*, 2021, 80(17), 581.

[21] M. Bhat, S. Han, and F. Porikli, Fast polar attentive 3D object detection on LiDAR point clouds, in *Proc. Machine Learning for Autonomous Driving Workshop*, Sydney, Australia, 2021.

[22] H. Li, G. Wu, S. Tao, H. Yin, K. Qi, S. Zhang, W. Guo, S. Ninomiya, and Y. Mu, Automatic branch-leaf segmentation and leaf phenotypic parameter estimation of pear trees based on three-dimensional point clouds, *Sensors*, 2023, 23(9), 4572.

[23] J. R. Rosell and R. Sanz, A review of methods and applications of the geometric characterization of tree crops in agricultural activities, *Comput. Electron. Agric.*, 2012, 81, 124–141.

[24] R. Sanz, J. R. Rosell, J. Llorens, E. Gil, and S. Planas, Relationship between tree row LiDAR-volume and leaf area density for fruit orchards and vineyards obtained with a LiDAR 3D dynamic measurement system, *Agric. For. Meteorol.*, 2013, 171–172, 153–162.

[25] G. Rivera, R. Porras, R. Florencia, and J. P. Sánchez-Solís, LiDAR applications in precision agriculture for cultivating crops: A review of recent advances, *Comput. Electron. Agric.*, 2023, 207, 107737.

[26] S. Jin, Y. Su, F. Wu, S. Pang, S. Gao, T. Hu, J. Liu, and Q. Guo, Stem-leaf segmentation and phenotypic trait extraction of individual maize using terrestrial LiDAR data, *IEEE Trans. Geosci. Remote Sens.*, 2019, 57(3), 1336–1346.

[27] A. Lau, L. P. Bentley, C. Martius, A. Shenkin, H. Bartholomeus, P. Raumonen, Y. Malhi, T. Jackson, and M. Herold., Quantifying branch

architecture of tropical trees using terrestrial LiDAR and 3D modelling, *Trees*, 2018, 32(5), 1219–1231.

[28] J. Murray, J. T. Fennell, G. A. Blackburn, J. D. Whyatt, and B. Li, The novel use of proximal photogrammetry and terrestrial LiDAR to quantify the structural complexity of orchard trees, *Precis. Agric.*, 2020, 21(3), 473–483.

[29] L. Wu, X. Zhu, R. Lawes, D. Dunkerley, and H. Zhang, Comparison of machine learning algorithms for classification of LiDAR points for characterization of canola canopy structure, *Int. J. Remote Sens.*, 2019, 40(15), 5973–5991.

[30] T. Medic, J. Bömer, and S. Paulus, Challenges and recommendations for 3D plant phenotyping in agriculture using terrestrial laser scanners, *ISPRS Ann. Photogramm. Remote Sens. Spatial Inf. Sci.*, 2023, X-1/W1-2023, 1007–1014.

[31] X. Ma, B. Wei, H. Guan, Y. Cheng, and Z. Zhuo, A method for calculating and simulating phenotype of soybean based on 3D reconstruction, *Eur. J. Agron.*, 2024, 154, 127070.

[32] H. Tang, S. Li, Z. Su, and Z, He, Cluster-based wood-leaf separation method for forest plots using terrestrial laser scanning data, *Remote Sens.*, 2024, 16(18), 3355.

[33] A. Zarei, B. Li, J. C. Schnable, E. Lyons, D. Pauli, K. Barnard, and B. Benes, PlantSegNet: 3D point cloud instance segmentation of nearby plant organs with identical semantics, *Comput. Electron. Agric.*, 2024, 221, 108922.

[34] X. Chen, S. Wen, L. Zhang, Y. Lan, Y. Ge, Y. Hu, and S. Luo, A calculation method for cotton phenotypic traits based on unmanned aerial vehicle LiDAR combined with a three-dimensional deep neural network, *Comput. Electron. Agric.*, 2025, 230, 109857.

[35] D. Xu, J. Zhu, and Y. Ma, Advancing sustainable solar greenhouse management through digital twin enabled by functional-structural plant modeling: Case study in Beijing, China, *Energy Convers. Manage.*, 2025, 346, 120505.

[36] N. Ariesen-Verschuur, C. Verdouw, and B. Tekinerdogan, Digital twins in greenhouse horticulture: A review, *Comput. Electron. Agric.*, 2022, 199, 107183.

[37] D. Xu, H. Chen, F. Ji, J. Zhu, Z. Wang, R. Zhang, M. Hou, X. Huang, D. Wang, T. Lu et al., New insights on canopy heterogeneous analysis and light micro-climate simulation in Chinese solar greenhouse, *Comput. Electron. Agric.*, 2025, 233, 110179.

[38] I. Hwang, S. Yoon, D. Kim, J. Kang, J. H. Kim, and J. E. Son, Evaluation of the effects of supplemental lighting and stem number on greenhouse sweet pepper growth and yield via ray-tracing simulation with 3D plant models, *Biosyst. Eng.*, 2023, 226, 252–265.

[39] Z. Wang, S. Xiao, Z. Miao, R. Liu, H. Chen, Q. Wang, K. Shao, R. Wang, and Y. Ma, P3DFusion: A cross-scene and high-fidelity 3D plant reconstruction framework empowered by vision foundation models and 3D Gaussian splatting, *Eur. J. Agron.*, 2025, 171, 127811.

Huayang Wang received the BS degree from China Agricultural University, Beijing, China, in 2025. She is currently pursuing the MS degree at School of Land Science and Technology, China Agricultural University, Beijing, China. Her research interests include 3D plant phenotyping and micro-climate characterization in solar greenhouses.

Jiayuan Li received the MS degree in computer science and technology from Jilin Agricultural University, China, in 2025. He is currently a research assistant at School of Land Science and Technology, China Agricultural University, China. His research interests include 3D reconstruction, robotics, and intelligent sensing technologies.

Maolin Hou received the MS degree in computer science and technology from China Agricultural University, China, in 2025. He is currently a research assistant at School of Land Science and Technology, China Agricultural University, China. His research interests include constructing crop models based on cucumber crop point clouds in solar greenhouses.

Yuntao Ma received the BS degree in computer and applied mathematics and the PhD degree in soil science from China Agricultural University, Beijing, China, in 2000 and 2006, respectively. She is currently a professor and doctoral supervisor at School of Land Science and Technology, China Agricultural University, China. Her research interests include system simulation and digital twins of plant function-structure-environment interactions, 3D plant phenotyping, agricultural applications of artificial intelligence, multi-sensor fusion, and digital agriculture.